


Low-cost dye-sensitized solar cells with ball-milled tellurium-doped graphene as counter electrodes and a natural sensitizer dye

Abdul Hai Alami^{1,2}  | Kamilia Aokal² | Di Zhang^{1,2} | Aya Taieb¹ | Mohammed Faraj² | Alya Alhammadi¹ | Juveiriah Mohammed Ashraf² | Bassel Soudan³  | Jinan El Hajjar¹ | Mihai Irimia-Vladu^{4,5}

¹Sustainable and Renewable Energy Engineering Department, University of Sharjah, PO Box 27272, Sharjah, United Arab Emirates

²Centre for Advanced Materials Research, University of Sharjah, PO Box 27272, Sharjah, United Arab Emirates

³Electrical and Computer Engineering Department, University of Sharjah, PO Box 27272, Sharjah, United Arab Emirates

⁴Institute of Physical Chemistry, Linz Institute for Organic Solar Cells (LIOS), Johannes Kepler University, Altenberger Str. Nr. 69, 4040 Linz, Austria

⁵Joanneum Research Forschungsgesellschaft mbH, Franz-Pichler Str. Nr. 30, 8160 Weiz, Austria

Correspondence

Abdul Hai Alami, Sustainable and Renewable Energy Engineering Department, University of Sharjah, PO Box 27272, Sharjah, United Arab Emirates. Email: aalalami@sharjah.ac.ae

Irimia-Vladu, Joanneum Research Forschungsgesellschaft mbH, Franz-Pichler Str. Nr. 30, 8160 Weiz, Austria. Email: mihai.irimia-vladu@joanneum.at

Funding information

University of Sharjah, Grant/Award Numbers: 1702040681-P and 1802040691-P; Sharjah Research Academy

Summary

This paper presents a facile and economic development of dye-sensitized solar cells using a nonprecious counter electrode made from ball-milled tellurium-doped graphene (Te-Gr) and a natural sensitizer extracted from *Calotropis gigantea* leaves. The prepared materials were characterized using various techniques, such as Raman spectroscopy, X-ray diffraction (XRD), atomic force microscopy (AFM), impedance spectroscopy, and scanning electron microscopy with built-in energy-dispersive X-ray spectroscopy (SEM with EDS). The electrochemical activity of the produced counter electrodes and the impedance of the fabricated cells were examined and discussed to devise plans for future enhancement of cell performance. A clear pattern of improvement was found when using cost-effective Te-Gr relative to the costly platinum counter electrodes, especially when compared with cells employing another natural sensitizer. The results show approximately 51% enhancement over chlorophyll-based cells made from spinach, where the added advantage in our approach is the utilization of an abundant plant extract with little nutritional appeal.

KEYWORDS

ball milling, dye-sensitized solar cells, low-cost counter electrodes, natural sensitizer, tellurium-doped graphene

1 | INTRODUCTION

According to the latest statistics by the Renewable Energy Policy Network (published in 2018), solar energy

presented the highest potential in terms of electricity generation (about 6.5 EJ) compared with all other energy sources, even conventional generation (about 3.7 EJ).¹ Given this huge potential, significant research effort has

been directed at improving the efficiencies and economics of harvesting energy from the sun, especially using photovoltaics.

The development of the solar photovoltaic cell has gone through three major phases of developments, dubbed solar cell generations.^{2,3} Silicon-based photovoltaics (PVs) comprise the first generation and account for almost 90% of the market share due to their high efficiency and long projected life.⁴ However, despite their popularity, silicon-based PVs are relatively expensive since they require significant amounts of energy to manufacture in the first place.^{5,6} To improve the economics, a second generation of solar cells based on thin film semiconductors has been developed. Their manufacturing is more cost-effective as they require less material.^{7,8} But, they exhibit lower efficiencies as compared with first-generation cells. A third generation of solar PV technology has come about with the long-term aim of achieving efficiency comparable with first-generation technology at the economics of second-generation manufacturing. The third generation of PV started with two developments at the beginning of the 1990s. Dye-sensitized solar cells (DSSCs) were demonstrated in 1991 with what became known as the Grätzel cell,⁹ and bulk heterojunction organic solar cells (OPVs) were demonstrated in 1992 by the group of Alan J. Heeger.¹⁰

Due to their production simplicity and benign components, DSSCs have received consistently increasing attention since their inception.¹¹⁻¹⁷ They completely eliminate the need for silicon and utilize various organic materials in their structures that can be obtained and manufactured at lower costs.

From the material point of view, DSSC's dependence on the expensive ruthenium (Ru)-based synthetic dyes and platinum (Pt)-based counter electrode poses a major disadvantage. Researchers have been experimenting with alternative materials that would meet the operational needs of the solar cells at lower costs and better efficiencies.^{18,19} Synthetic Ru-based dyes could be replaced by low-cost dyes with natural origins, albeit typically showing lower performance [cite several sources]. The cost of the counter electrode may be reduced by adopting low-cost carbon-based materials. Jeon et al, for example, have demonstrated a novel counter electrode material based on ball-milled metalloid tellurium-doped graphene nanoplatelets.¹⁸ While the results showed comparable performances to the reference Pt leading to strong evidence of design practicality and cell durability, the ball-milled product required a heavy wet chemical purifying process to remove unreacted tellurium and metal impurities before cell assembly. Ju et al used a similar approach by employing edge-selenated graphene counter electrodes for the same purpose of replacing the Pt counter

electrode.²⁰ The selenium is used in place of the tellurium reported in the work of Jeon et al,²¹ and the reported efficiency for the selenated graphene outperformed the Pt-based counter electrodes.

This work presents a low-cost process to synthesize DSSC tellurium-based counter electrodes, with the use of the natural sensitizer *chlorophyll* extracted from the *Calotropis gigantea* plant. This plant was selected due to its high efficiency of extraction and its abundance in the host country, the United Arab Emirates.^{22,23} It has been shown that natural sensitizers in general exhibit low photoelectric conversion efficiency—spinach has been shown to have a conversion efficiency of only 0.278%, *Ipomoea* leaf an efficiency of 0.318%,²⁴ and the fruits such as the St. Lucie cherry has been shown to produce a power conversion efficiency of 0.19% (under 0.3-sun conditions).²⁵ While this is low in comparison with efficiencies of synthetic dyes (7% to 8% efficiency), one needs to take into consideration the cost of production and the environmental effects of the synthetic dyes. Furthermore, we aim to include cost-effective Pt-free counter electrode with ease of preparation. Ball-milled tellurium-doped graphene (Te-Gr) is selected due to their low overall cost, good electrical conductivity, and excellent catalytic activity. In contrast, we will demonstrate a simple dry ball-milling process without the need for wet chemical treatments. Thus, the objective is to propose a combination of facile preparation and low-cost counter electrode with the utilization of a natural sensitizer and assess their contribution to the promotion of practical applications of DSSCs as green alternatives to silicon and other costly synthetic organic materials.^{26,27}

2 | EXPERIMENTAL WORK

2.1 | Dye extraction and optical characterization

For dye extraction and preparation, 15 g of *C. gigantea* leaves was thoroughly cleaned with deionized water, cut into small pieces, and placed in a beaker with 45 mL of ethanol (enough to cover the surface of the leaves). Then, 0.0883 g of chenodeoxycholic acid from Solaronix was added to the solution to prevent dye aggregation. The beaker was then sealed tightly with parafilm and placed in an ultrasonic bath for 30 minutes. To maintain consistency, the solution was filtered using PTEF syringe of 0.45- μ m pores and was stored in the dark to prevent dye oxidation.

The optical absorbance of the dye solution was carried out by placing the dye in transparent cuvettes (Ocean Optics Ultra Micro Cell with a range of 220-900 nm) on

cuvette holder, and the measurements were done via a Maya 2000-Pro high-resolution spectrometer (Ocean Optics) with a HL-2000 tungsten halogen light source. To measure the UV-to-infrared spectrum range (wavelength range from 200 to 1100 nm with 0.2-nm resolution), three Maya 2000 spectrometers were used with software signal stitching.

2.2 | Electrode preparation

We prepared tellurium-based experimental electrodes and Pt-based control electrodes for comparison. The experimental and control cells were evaluated and compared in terms of their electrical and electrochemical characteristics. The following subsections detail the preparation process for the electrodes.

2.2.1 | Synthesis of Te-Gr powder

We applied a single-step synthesis of tellurium-doped graphene nanoplatelets (Te-Gr) without further purification processes. The material for obtaining tellurium-doped graphene was processed by adding 5.0-g high-purity graphite of particle sizes less than 125 μm (obtained from Emirates Steel, United Arab Emirates) to 5.0 g of tellurium powder (with a purity of 99.99%, 325 mesh from Alibaba.com) and ball milling the mixture in a 25-mL stainless steel crucible with 5-mm stainless steel balls for 48 hours at 500 rpms.

2.2.2 | Photoelectrode preparation

Ready-made photoelectrodes, purchased from Solaronix, were composed of $2 \times 2 \text{ cm}^2$ fluorine-doped tin oxide (FTO) substrates coated with $0.6 \times 0.6 \text{ cm}^2$ transparent (10- μm thickness) and opaque titanium dioxide (TiO_2) with a thickness of 2 μm . The substrates were heated at 773 K (500°C) for 40 minutes then left to cool to around 323 K (50°C) before being immersed in the *C. gigantea* dye solution overnight. After the staining process, the *C. gigantea* dye-soaked titania electrodes were rinsed in ethanol and left to dry at room temperature.

2.2.3 | Counter electrode preparation

Te-Gr was processed from solution and cast over an FTO electrode to create the Te-Gr counter electrodes. The electrodes were prepared by mixing 50 mg of Te-Gr powder with 100 μL of Nafion dispersion purchased from the Fuel Cell Store. Seven hundred fifty microliters of 2-propanol and 2750 μL of deionized water were then

added to the mixture and were sonicated for 30 minutes in an ultrasonic bath. An FTO of $2 \times 2 \text{ cm}^2$ in size was also cleaned with ethanol in an ultrasonic bath for 30 minutes before drop casting 400 μL of the Te-Gr solution. The substrates were then left to dry at 313 K (40°C) before assembly. Ready-made $2 \times 2 \text{ cm}^2$ Pt electrodes also purchased from Solaronix and used as the control counter electrodes. Both types of counter electrodes were heated at 393 K (120°C) for 15 minutes before assembly, in order to remove any buildup of moisture.

2.3 | Counter electrode characterization

Several characterization experiments were conducted on the counter electrodes before the DSSC was assembled and tested. The counter electrodes were put through Raman measurements as well as scanning electron microscopy-energy-dispersive X-ray spectroscopy (SEM-EDS) to ascertain the formation of the Te-Gr layer as expected. The Raman spectra were measured with a Renishaw in Via Raman microscope with a visible 514-nm laser. SEM-EDS was performed at $\times 7000$ and $\times 500$ magnifications, 20.0 kV accelerating voltage, and a working distance of 13.7 mm. The electrochemical properties of the counter electrodes were then characterized through cyclic voltammetry and impedance spectroscopy.

2.4 | DSSC assembly and I-V measurements

A Meltonix sealing film gasket was placed around each active area of titania electrode, and the space was filled with Iodolyte AN-50 electrolyte. The electrodes were then assembled together using binder clips for testing. Each assembled DSSC was tested under an ABET SunLite sun simulator using a PC-interfaced Keithley 2400 SourceMeter. A schematic of a DSSC cell is shown in Figure 1.

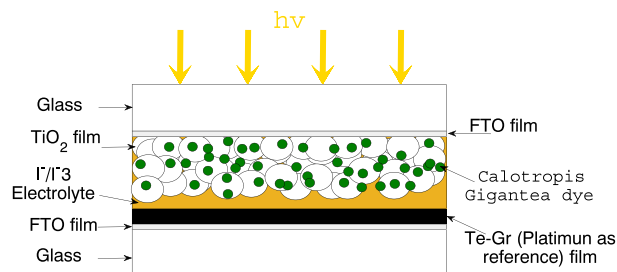


FIGURE 1 The dye-sensitized solar cell (DSSC) setup employed in this work [Colour figure can be viewed at wileyonlinelibrary.com]

3 | RESULTS AND DISCUSSION

3.1 | Raman characterization of the Te-Gr counter electrode

The structures of pure graphite powder as a reference and the sample Te-Gr deposited on FTO were studied using Raman spectroscopy as doping in graphene will affect the expected coupling between the electrons generated by incident phonons.²⁸ In comparison with graphite, the samples indicate the presence of multilayer graphene, as seen in Figure 2. This is shown with respect to the shift in G band shape and position occurring at higher frequencies as doping causes the relaxation of sp^2 bonds which in turn are more capable of an increase in energy.

Pristine graphite exhibited a sharp G band with a low I_D/I_G ratio due to its large grain size (in excess of $63 \mu\text{m}$ after the sieving process during graphite preparation) and well-ordered graphitic structure. Crystallite sizes (L_a) shown in Table 1 were calculated from the following equation:

$$C_a = (2.4 \times 10^{-10}) \lambda^4_{\text{laser}} I_D / I_G^{-1} \quad (1)$$

Edge functionalization of graphene, on the other hand, exhibited an apparent change in G-band shape and position and a much larger I_D/I_G ratio with the latter being

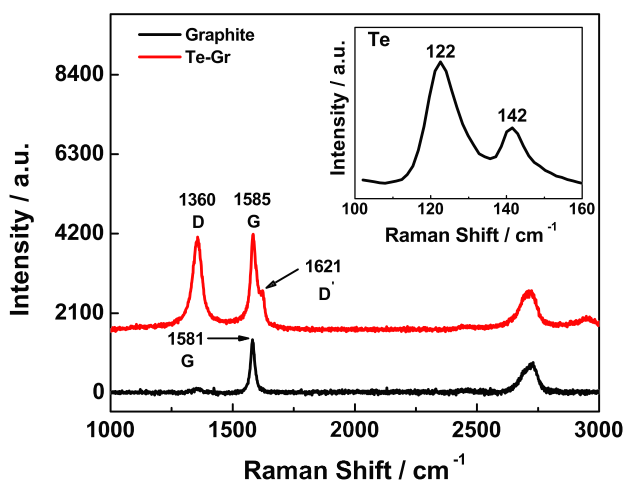


FIGURE 2 Comparison of the Raman spectra for graphite and Te-Gr powders. The inset shows the Raman spectra of tellurium at a lower range of frequency [Colour figure can be viewed at wileyonlinelibrary.com]

TABLE 1 Summary for graphite and Te-Gr Raman parameters

Sample	$(I_D/I_G)^{-1}$	L_a , nm
Graphite powder	1.85	30.91
Te-Gr sample	0.97	16.32

indicative of a small resulting crystallite size as shown in Table 1. A D' band occurring at 1623 cm^{-1} along with the D band (1357 cm^{-1}) is strongly suggestive of edge functionalization.²¹ Peaks occurring at lower frequencies are indicative of tellurium and occur due to the lattice vibrations of its trigonal lattice structure.²⁹

3.2 | Scanning electron microscopy of the Te-Gr counter electrode

SEM-EDS results reveal the homogeneity of tellurium interdiffusion into the graphene. Figure 3A,B shows the highly porous structure of Te-Gr with the presence of agglomerated spherical-shaped particles with size ranges from 1 to $3 \mu\text{m}$. Pristine graphite used in the experiments had a large particle size distribution ($63 < x < 125 \mu\text{m}$) obtained from sieved powdered graphite. After ball milling, it is observed that the particle size of resultant Te-Gr powder was dramatically reduced which implies a mechanical exfoliation reaction of the graphite powder.

The EDS element content by volume shown in Figure 3C to 3E depicts the content of tellurium to be 64.4 wt%, while the content of carbon was found to be 21.8 wt%, and a 10.5 wt% of oxygen was present from the surrounding environment. Map spectrum of Figure 3C shows the existence of a high percentage of tellurium indicating the presence of the unreacted tellurium attached to the surface of the substrate.

3.3 | Electrochemical characterization of the Te-Gr counter electrode

To examine the catalytic activity, cyclic voltammetry (CV) and electrochemical impedance spectroscopy (EIS) were performed using the VP300 potentiostat from Bio-Logic.

3.3.1 | Cyclic voltammetry

CV was done with a three-electrode setup where the sample was a working electrode, a saturated calomel electrode (SCE) acted as the reference electrode while a platinum wire was used as the counter electrode. The electrolyte was comprised of 10 mM of lithium iodide (LiI), 1 mM iodine crystals (I_2), and 0.1M of lithium perchlorate (LiClO_4) in acetonitrile solution. The scan rate was fixed at 20 mVs^{-1} .

Two pairs of redox reaction peaks can be seen from the CV scan in Figure 4 for current density vs working electrode potential for both the Pt and Te-Gr electrodes. The pairs of peaks conform to the following redox equations, respectively:

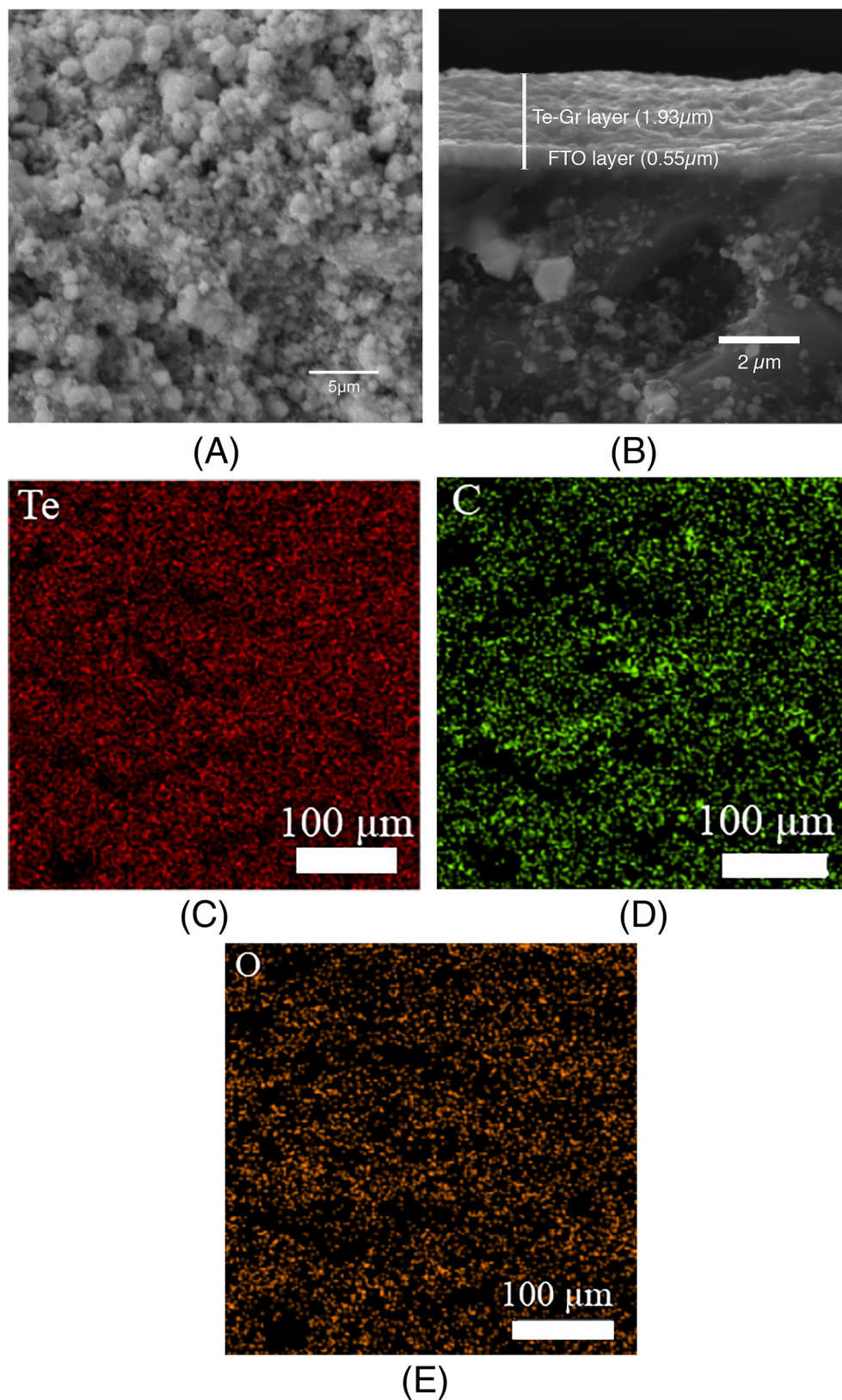


FIGURE 3 SEM image of the tellurium-doped graphene films at A, $\times 7000$ magnification and B, its cross-sectional area at $\times 20\,000$ magnification with corresponding EDS maps for C, tellurium, D, carbon, and E, oxygen [Colour figure can be viewed at wileyonlinelibrary.com]

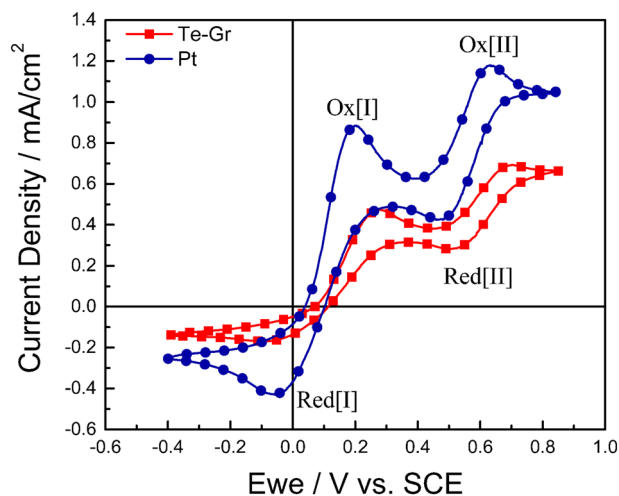
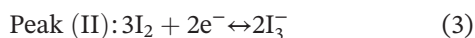
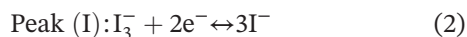


FIGURE 4 Cyclic voltammetry spectra of sample showing redox couple iodide/triiodide peaks [Colour figure can be viewed at wileyonlinelibrary.com]



In DSSCs, the reaction occurring at the counter electrode is responsible for the catalysis of the reduction reaction of I_3^- into I^- , and hence, our main focus is on the first occurring redox reaction (I).

Reduction reactions occur at 520 and -60 mV for Te-Gr while reduction peaks for the Pt electrode appear at 500 and -60 mV. At the same time, oxidation reactions occur at 650 and 250 mV for Te-Gr and at 600 and 200 mV for the Pt electrode. From Figure 4, it is clearly shown that the Te-Gr sample depicts a reduced ability to maintain energy and thus could speed up the transfer of energy for a faster charge/discharge cycle of the iodolyte but at the cost of efficient transfer. The CV readings have been acquired over 11 cycles, and good stability has been obtained for both working electrodes after a maximum of three consecutive cycles. The effect of hysteresis is not seen to be a limiting factor to the obtained results. It should be mentioned that the Te-Gr is thicker due to the synthesis technique of drop casting that usually produces thicker deposits than screen printing, the process used to apply Pt on FTO. Both samples show low values of current density for reduction peaks occurring in the negative quadrant which could be due to an active area that may have been too large ($1 \text{ cm} \times 2 \text{ cm}$). The analyte must diffuse into the working electrode for a redox reaction to occur which can limit the current of the reaction. We infer that the low values obtained for the current density, on the other hand, could be attributed to the effect that the excess tellurium had on the electrode where

electrons are trapped. Or, on the other hand, could be attributed to dissolved oxygen ions from the surrounding atmosphere that lead to iodide ions losing electrons, therefore causing a buildup of I^- ions on the electrode. As tellurium enhances the spectral response at long wavelengths in the visible region due to increased photogeneration efficiency, continuous heat from the sun simulator stimulated electrocatalysis on the counter electrode in the assembled solar cell.³⁰ Nafion, an acidic binding agent, could also be attributed as a cause for low current density values. It acts as a proton conductor and may not allow electrons to reach either the tellurium or the Te-Gr-coated counter electrode to allow for electrolyte reduction depending on whichever one it is bound to, ie, it acts as an electrical insulator.

3.3.2 | Electrical impedance spectroscopy spectra—Nyquist plot

Impedance spectroscopy helps in understanding the processes that occur at interfaces, especially the changes in physical properties of the system (ie, crystallographic, mechanical, compositional, or electrical). It also helps in understanding changes in electrical properties of, ie, polarization by studying their effect on the electrical conductivity of the system.^{20,21,31-34} Impedance spectroscopy offers the advantage that the conductivity measurement is taken over a range of frequencies. This can allow for obtaining information on the different conductive species and pathways. These pieces of information are important in understanding and controlling the conduction mechanism.

We performed impedance spectroscopy on Te-Gr on FTO glass electrodes and compared it with the spectra recorded from Pt electrodes. Symmetrical sandwich-typed dummy cells were fabricated with two identical Pt electrodes and two identical Te-Gr electrodes on FTO glass, which were separated by a Meltonix sealant and spacer exposing a $0.8 \text{ cm} \times 0.8 \text{ cm}$ active area. The spacer was filled with Iodolyte AN-50 electrolyte, and the EIS spectra were attained in the frequency range from 1 MHz to 0.1 Hz at 0 V open-circuit voltage with the AC modulation amplitude set at 10 mV.

The EIS spectra of the Pt-coated electrode (inset in Figure 5) exhibited two semicircles that correspond to a charge transfer process and Nernst diffusion appearing at high and low frequencies, respectively. The figure also shows that the Te-Gr sample substrate in I^-/I_3^- electrolytes has shown the three semicircles that are expected when testing highly porous carbon materials. The electrolyte contact resistance, the first x-axis intercept, of Te-Gr (40Ω) was high compared with the 17Ω of the Pt

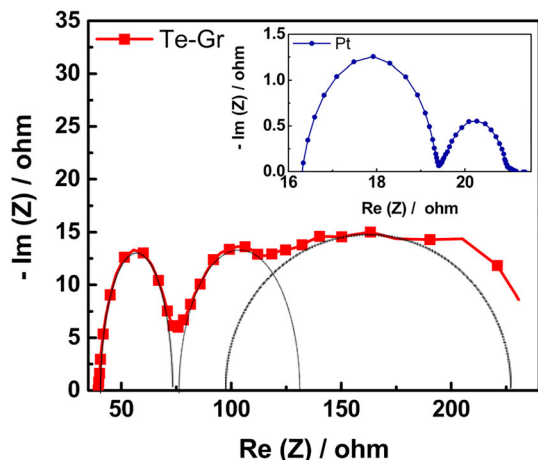


FIGURE 5 Nyquist plot of Te-Gr counter electrodes in the dark. The inset shows a comparison with Pt working electrode [Colour figure can be viewed at wileyonlinelibrary.com]

reference electrode. This could possibly be attributed to weak electrolyte adsorption. The charge transfer resistance (R_{ct}) provides a good reasoning for electrocatalytic activity. The charge transfer resistance for the Te-Gr substrate, however, was higher than its Pt counterpart, even when the tests are repeated under 1-sun light conditions as seen in Figure 6.

There is also clear evidence that series resistance of the Te-Gr electrode is high as seen from the I-V curves in later sections due to the nature of bulk deposition. The charge transfer resistance (R_{ct}) for the tested Te-Gr electrodes indicates a relatively large reaction velocity of the Γ^-/Γ^{3-} regeneration at their surface. In the solar cell, it performed better—but with a limited output—because there was a flow of current throughout with pathways for the current through the cell caused by impurities. In our case, this may have been due to a high percentage

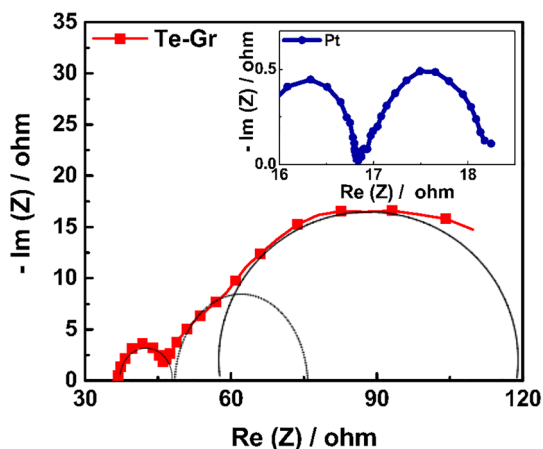


FIGURE 6 Nyquist plot of Te-Gr counter electrodes under 1-sun light conditions. The inset shows a comparison with Pt working electrode [Colour figure can be viewed at wileyonlinelibrary.com]

of Te in the powder during the manufacturing process that may have adhered to the TiO_2 during the cell assembly process as tellurium enhances the spectral response at long wavelengths.³⁰

3.4 | Optical characterization of the dye

Following the chlorophyll dye extraction from *C. gigantea* leaves, an optical assessment was conducted by applying the dye on a photoelectrode (FTO with TiO_2 deposit). Figure 7 shows the absorbance results of the substrate soaked with the chlorophyll pigment source compared with a bare TiO_2 reference. The bandgaps are also calculated and shown in the inset.

The absorbance curves show the expected higher spectral absorbance at the visible region for the *C. gigantea* dye, with both electrodes leveling off at the edge of the near infrared region. This has a noticeable effect in enhancing cell performance with less heat-generating radiation being absorbed into the photoelectrode. The extracted dye solution has been evaluated optically as seen in Figure 8 below.

The effective absorption range of the dye is centered around the 630 to 690 nm range, with a wide peak at 658 nm. The absorption falls sharply at the threshold of the near-infrared range. The broad peak, dominating the absorptivity spectrum, ranging from 649 to 675 nm corresponds to two absorption peaks with similar intensities of *chlorophyll A* and *B*, both of which occur at wavelengths of around 650 and 675 nm in ethanol, respectively. The reason they occur with the same intensity could be due to the fact that chlorophyll B is more soluble in polar substances than chlorophyll A. Other absorptivity peaks occurring at 625 and 580 nm also

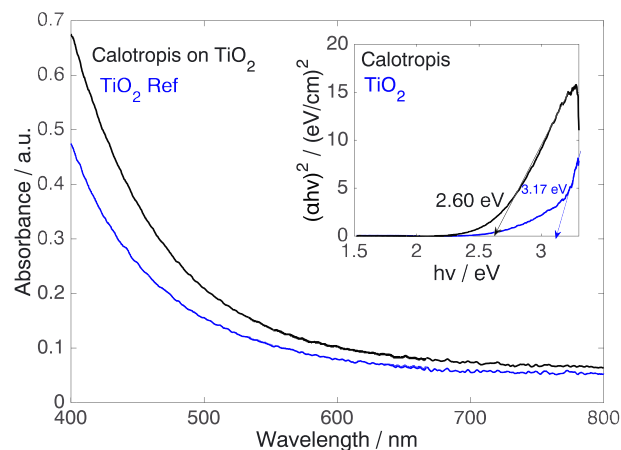


FIGURE 7 Spectral absorbance of *Calotropis gigantea* dye compared with a bare titania photoelectrode. The bandgaps (inset) are calculated via Tauc formula [Colour figure can be viewed at wileyonlinelibrary.com]

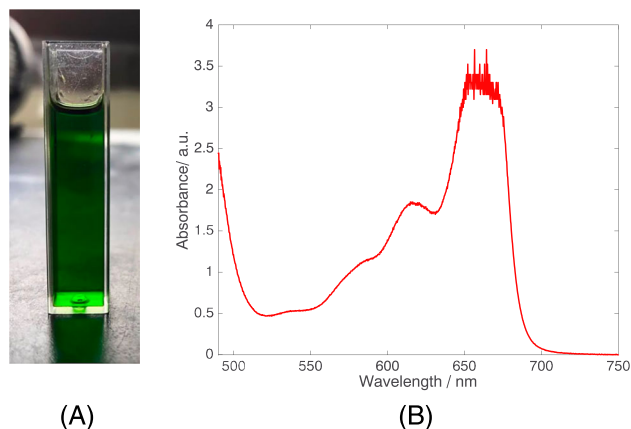


FIGURE 8 A, Chlorophyll extract from *Calotropis gigantea* dissolved in ethanol. B, The corresponding absorbance spectrum [Colour figure can be viewed at wileyonlinelibrary.com]

correspond to chlorophyll as it is the primary photosynthetic pigment of *Calotropis*.³⁵

3.5 | I-V characteristic curves of the DSSC

Figure 9 depicts the cell characteristics of current density-voltage curves along with other pertinent PV parameters.

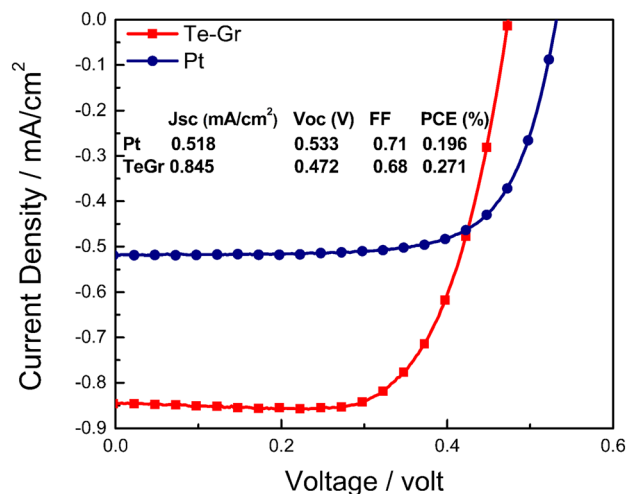


FIGURE 9 Current density-voltage (J-V) characteristics of *Calotropis* dye-sensitized solar cells (DSSCs) using platinum (blue) and Te-Gr counter electrodes (red). The inset table shows the efficiency and other parameters for respective cells [Colour figure can be viewed at wileyonlinelibrary.com]

The Te-Gr solar cell clearly exhibits better performance compared with the cell parameters obtained with a Pt electrode, suggesting noticeable electrical enhancement.

The short-circuit current density (J_{SC}) of the Te-Gr cell increased by 0.33 mA/cm² compared with the Pt reference cell as the open circuit voltage (V_{OC}) decreased by 0.06 V. The lower V_{OC} in the Te-Gr cell is a result of the positively shifted half-wave redox potential compared with the Pt cell³⁶ as extracted from the CV spectra in Figure 4, which are 94 and 73 mV for Te-Gr and Pt, respectively. The fill factor (FF) of the Te-Gr cell was around 3% higher than that of the Pt reference cell, thus suggestive of a better cell performance. This was indicated by an increase of around 28% in power conversion efficiency (PCE) of the Te-Gr DSSCs. We rationalize that adsorbance of iodide ions onto the unreactive tellurium could have caused the limited increase in conductivity that occurred with the increase in the active surface area. The same observation is reported in the work of Jeon et al, where they reported a current density value of 15 mA cm⁻².²¹ On the other hand, an increase in series resistance is visible with a lower FF than should have been achieved. This is mainly attributed to the high percentage of unreacted Te of the bulk thus reducing the active surface area of the Te-Gr substrate. Another contribution to the limited current increase could be the existence of remnants of the Nafion used for particle suspension as it acts as an electronic insulator. The open circuit voltage, however, changed due to a varying difference between the Fermi level of TiO₂ with the impurities/Te-Gr or Te particles available from the counter electrode that passed through the electrolyte ending up at the photoelectrode and the oxidation-reduction potential change of electrolyte. The details of the characteristics of the produced cells are shown in the inset of Figure 9, and also in Table 2, with a comparison of a naturally (chlorophyll) sensitized cell by Chang et al.²⁴ The efficiency of the cell shows around 51% increase in the efficiency over a similarly sensitized cell. In general, the efficiency of cells sensitized by natural dyes is low (less than 1%) in most of the reviewed literature.³⁷⁻⁴⁴ The main advantage of the work reported here is twofold: First, the sensitizer is a nonfood material, and second, it is expected that the dyes extracted from the plants will change with seasons to control the amount of radiation absorbed by

TABLE 2 Summary of characteristics of the produced cells compared with a reported Pt-based chlorophyll cell²⁴

Cell (Sensitizer/CE)	J_{SC} , mA cm ⁻²	V_{OC} , V	FF	PCE, %
<i>Calotropis</i> /Pt	0.518	0.533	0.71	0.196
<i>Calotropis</i> /Te-Gr	0.845	0.472	0.68	0.271
Spinach/Pt (reported) ²⁴	0.55	0.467	0.51	0.131

the plant (lighter dye colors in summer absorb less than richer colors in winter) and thus can mitigate efficiency loss due to heating in summer and due to lack of solar irradiation in winter.

4 | CONCLUSIONS

We demonstrated here the feasibility to fabricate DSSC based on plant pigments as sensitizers and Te-Gr composite as counter electrode material. The counter electrode manufacturing was based on centrifugal milling, to produce the tellurium-activated graphene that was deposited on FTO and compared with a Pt counter electrode. The assembled Te-Gr-based cells have shown an efficiency enhancement of around 28% compared with reference cells that have Pt as their working electrode. The natural sensitizer (dye) used comes from *C. gigantea*, a plant that is ideal for such applications as it is native to the research geographical location and is not used as a food item for people or livestock. This work paves the way for further optimization of Te-Gr composition and deposition as an alternative counter electrode material for natural DSSCs. The results show approximately 51% enhancement over chlorophyll-based cells made from spinach, where the added advantage in our approach is the utilization of an abundant plant extract with little nutritional appeal. Our future work will focus on identifying better natural sensitizers and improving the cell geometry, in order to extract the true potential of Te-Gr for DSSC counter electrode fabrication, and the results will be part of a follow-up publication.

ACKNOWLEDGEMENTS

The authors would like to acknowledge the technical assistance of Dr Mohammed Ali Abdelkareem from The Sustainable and Renewable Energy Engineering Department of the University of Sharjah. This project is funded by the University of Sharjah under grants 1702040681-P and 1802040691-P.

ORCID

Abdul Hai Alami  <https://orcid.org/0000-0001-9986-4324>
Bassel Soudan  <https://orcid.org/0000-0001-8128-5498>

REFERENCES

- Photovoltaic research. <https://www.nrel.gov/pv/>. Accessed February 20, 2019.
- Green MA, Hishikawa Y, Dunlop ED, Levi DH, Hohl-Ebinger J, Ho-Baillie AWY. Solar cell efficiency tables (version 51). *Prog Photovoltaics Res Appl*. 2018;26(1):3-12. <https://doi.org/10.1002/pip.2978>
- NREL. NREL efficiency chart. <https://www.nrel.gov/pv/assets/pdfs/pv-efficiencies-07-17-2018.pdf>. Published 2018. Accessed December 15, 2018.
- Polman A, Knight M, Garnett EC, Ehrler B, Sinke WC. Photovoltaic materials: present efficiencies and future challenges. *Science (80-)*. 2016;352(6283):4424-4424. <https://doi.org/10.1126/science.aad4424>
- Wu J, Lan Z, Lin J, et al. Electrolytes in dye-sensitized solar cells. *Chem Rev*. 2015;115(5):2136-2173. <https://doi.org/10.1021/cr400675m>
- Sherwani AF, Usmani JA, Varun. Life cycle assessment of solar PV based electricity generation systems: a review. *Renew Sustain Energy Rev*. 2010;14(1):540-544. <https://doi.org/10.1016/J.RSER.2009.08.003>
- Hosenuzzaman M, Rahim NA, Selvaraj J, Hasanuzzaman M, Malek ABMA, Nahar A. Global prospects, progress, policies, and environmental impact of solar photovoltaic power generation. *Renew Sustain Energy Rev*. 2015;41:284-297. <https://doi.org/10.1016/J.RSER.2014.08.046>
- Ghosh KK. *Status and technology of present day solar cells*. In: Springer, Singapore; 2017:19-28. https://doi.org/10.1007/978-981-10-3908-9_3
- O'Regan B, Grätzel M. A low-cost, high-efficiency solar cell based on dye-sensitized colloidal TiO₂ films. *Nature*. 1991; 353(6346):737-740. <https://doi.org/10.1038/353737a0>
- Sariciftci NS, Smilowitz L, Heeger AJ, Wudl F. Photoinduced electron transfer from a conducting polymer to Buckminsterfullerene. *Science (80-)*. 1992;258(5087):1474-1476. <https://doi.org/10.1126/science.258.5087.1474>
- PhysOrg.com. Sanyo announces world's most efficient solar module. <https://phys.org/news/2010-06-sanyo-world-efficient-solar-module.html>. Accessed December 20, 2019.
- Janssen RAJ, Nelson J. Factors limiting device efficiency in organic photovoltaics. *Adv Mater*. 2013;25(13):1847-1858. <https://doi.org/10.1002/adma.201202873>
- Balasingam SK, Lee M, Kang MG, Jun Y. Improvement of dye-sensitized solar cells toward the broader light harvesting of the solar spectrum. *Chem Commun*. 2013;49(15):1471-1487. <https://doi.org/10.1039/C2CC37616D>
- Xie K, Guo M, Huang H. Photonic crystals for sensitized solar cells: fabrication, properties, and applications. *J Mater Chem C*. 2015;3(41):10665-10686. <https://doi.org/10.1039/C5TC02121A>
- Pazoki M, Cappel UB, Johansson EMJ, Hagfeldt A, Boschloo G. Characterization techniques for dye-sensitized solar cells. *Energ Environ Sci*. 2017;10(3):672-709. <https://doi.org/10.1039/C6EE02732F>
- Singh E, Kim KS, Yeom GY, Nalwa HS. Two-dimensional transition metal dichalcogenide-based counter electrodes for dye-sensitized solar cells. *RSC Adv*. 2017;7(45):28234-28290. <https://doi.org/10.1039/C7RA03599C>
- Benesperi I, Michaels H, Freitag M. The researcher's guide to solid-state dye-sensitized solar cells. *J Mater Chem C*. 2018;6(44):11903-11942. <https://doi.org/10.1039/C8TC03542C>
- Ngidi NPD, Ollengo MA, Nyamori VO. Heteroatom-doped graphene and its application as a counter electrode in dye-sensitized solar cells. *Int J Energy Res*. 2019;43(5):1702-1734. <https://doi.org/10.1002/er.4326>

19. Cruz R, Brandão L, Mendes A. Use of single-wall carbon nanohorns as counter electrodes in dye-sensitized solar cells. *Int J Energy Res.* 2013;37(12):1498-1508. <https://doi.org/10.1002/er.2959>
20. Ju MJ, Jeon I-Y, Kim HM, et al. Edge-selenated graphene nanoplatelets as durable metal-free catalysts for iodine reduction reaction in dye-sensitized solar cells. *Sci Adv.* 2016;2(6):e1501459. <https://doi.org/10.1126/sciadv.1501459>
21. Jeon I-Y, Kim HM, Kweon DH, et al. Metalloid tellurium-doped graphene nanoplatelets as ultimately stable electrocatalysts for cobalt reduction reaction in dye-sensitized solar cells. *Nano Energy.* 2016;30:867-876. <https://doi.org/10.1016/J.NANOEN.2016.09.001>
22. Alami AH, Aokal K, Zhang D, Tawalbeh M, Alhammadi A, Taieb A. Assessment of Calotropis natural dye extracts on the efficiency of dye-sensitized solar cells. *Agron Res.* 2018;16(4):1569-1579. <https://doi.org/10.15159/AR.18.166>
23. Zhang D, Alami AH, Tawalbeh M, et al. Efficiency and high-temperature response of dye-sensitized solar cells using natural dyes extracted from Calotropis. In: *2018 5th International Conference on Renewable Energy: Generation and Applications (ICREGA)*. IEEE; 2018:183-187. <https://doi.org/10.1109/ICREGA.2018.8337593>
24. Chang H, Wu HM, Chen TL, Huang KD, Jwo CS, Lo YJ. Dye-sensitized solar cell using natural dyes extracted from spinach and ipomoea. *J Alloys Compd.* 2010;495(2):606-610. <https://doi.org/10.1016/J.JALLCOM.2009.10.057>
25. Atli A, Atilgan A, Altinkaya C, Ozel K, Yildiz A. St. Lucie cherry, yellow jasmine, and madder berries as novel natural sensitizers for dye-sensitized solar cells. *Int J Energy Res* June 2019;43(825):3914-3922. er.4538. <https://doi.org/10.1002/er.4538>
26. Gutowski TG, Branham MS, Dahmus JB, Jones AJ, Thiriez A, Sekulic DP. Thermodynamic analysis of resources used in manufacturing processes. *Environ Sci Technol.* 2009;43(5):1584-1590. <https://doi.org/10.1021/es8016655>
27. Irimia-Vladu M. "Green" electronics: biodegradable and biocompatible materials and devices for sustainable future. *Chem Soc Rev.* 2014;43(2):588-610. <https://doi.org/10.1039/C3CS60235D>
28. Yan J, Zhang Y, Kim P, Pinczuk A. Electric field effect tuning of electron-phonon coupling in graphene. *Phys Rev Lett.* 2007;98(16):166802. <https://doi.org/10.1103/PhysRevLett.98.166802>
29. Pine AS, Dresselhaus G. Raman spectra and lattice dynamics of tellurium. *Phys Rev B.* 1971;4(2):356-371. <https://doi.org/10.1103/PhysRevB.4.356>
30. Park W-D, Tanioka K. Tellurium doping effect in avalanche-mode amorphous selenium photoconductive film. *Appl Phys Lett.* 2014;105(19):192106. <https://doi.org/10.1063/1.4902011>
31. Suhaimi S, Shahimin M, Alahmed ZA, Chyský J, Reshak AH. *Materials for Enhanced Dye-Sensitized Solar Cell Performance: Electrochemical Application*. Vol 10.; 2015. www.electrochemsci.org. Accessed February 27, 2019.
32. Macdonald JR, James R. *Impedance Spectroscopy: Emphasizing Solid Materials and Systems*. Wiley; 1987. https://books.google.ae/books/about/Impedance_Spectroscopy.html?id=hblpQgAACAAJ&redir_esc=y. Accessed February 27, 2019.
33. Irimia-Vladu M, Fergus JW. Impedance spectroscopy of thin films of emeraldine base polyaniline and its implications for chemical sensing. *Synth Met.* 2006;156(21-24):1396-1400. <https://doi.org/10.1016/J.SYNTHMET.2006.11.004>
34. Irimia-Vladu M, Marjanovic N, Bodea M, et al. Small-molecule vacuum processed melamine-C60, organic field-effect transistors. *Org Electron.* 2009;10(3):408-415. <https://doi.org/10.1016/J.ORGEL.2009.01.002>
35. DHI. C14 - DHI LAB products and related services. <http://c14.dhigroup.com>. Accessed December 15, 2018.
36. Dao V-D, Kim S-H, Choi H-S, Kim J-H, Park H-O, Lee J-K. Efficiency enhancement of dye-sensitized solar cell using Pt hollow sphere counter electrode. *J Phys Chem C.* 2011;115(51):25529-25534. <https://doi.org/10.1021/jp208295b>
37. Prabavathy N, Shalini S, Balasundaraprabhu R, Velauthapillai D, Prasanna S, Muthukumarasamy N. Enhancement in the photostability of natural dyes for dye-sensitized solar cell (DSSC) applications: a review. *Int J Energy Res.* 2017;41(10):1372-1396. <https://doi.org/10.1002/er.3703>
38. Prabavathy N, Shalini S, Balasundaraprabhu R, et al. Algal buffer layers for enhancing the efficiency of anthocyanins extracted from rose petals for natural dye-sensitized solar cell (DSSC). *Int J Energy Res.* 2018;42(2):790-801. <https://doi.org/10.1002/er.3866>
39. Kavitha S, Praveena K, Lakshmi M. A new method to evaluate the feasibility of a dye in DSSC application. *Int J Energy Res.* 2017;41(14):2173-2183. <https://doi.org/10.1002/er.3778>
40. Kojima A, Teshima K, Shirai Y, Miyasaka T. Organometal halide perovskites as visible-light sensitizers for photovoltaic cells. *J Am Chem Soc.* 2009;131(17):6050-6051. <https://doi.org/10.1021/ja809598r>
41. Brabec CJ, Gowrisanker S, Halls JJM, Laird D, Jia S, Williams SP. Polymer-fullerene bulk-heterojunction solar cells. *Adv Mater.* 2010;22(34):3839-3856. <https://doi.org/10.1002/adma.200903697>
42. Dennler G, Scharber MC, Brabec CJ. Polymer-fullerene bulk-heterojunction solar cells. *Adv Mater.* 2009;21(13):1323-1338. <https://doi.org/10.1002/adma.200801283>
43. Koster LJA, Shaheen SE, Hummelen JC. Pathways to a new efficiency regime for organic solar cells. *Adv Energy Mater.* 2012;2(10):1246-1253. <https://doi.org/10.1002/aenm.201200103>
44. Yoshikawa K, Kawasaki H, Yoshida W, et al. Silicon heterojunction solar cell with interdigitated back contacts for a photoconversion efficiency over 26%. *Nat Energy.* 2017;2(5):17032. <https://doi.org/10.1038/nenergy.2017.32>

How to cite this article: Alami AH, Aokal K, Zhang D, et al. Low-cost dye-sensitized solar cells with ball-milled tellurium-doped graphene as counter electrodes and a natural sensitizer dye. *Int J Energy Res.* 2019;43:5824–5833. <https://doi.org/10.1002/er.4684>